Reentrant paramagnetism induced by drastic reduction of magnetic couplings at surfaces of superparamagnetic nanoparticles

Wei Qin,[1] Xiaoguang Li,[1,2] Yi Xie,[3] and Zhenyu Zhang[1,*]

[1]*International Center for Quantum Design of Functional Materials (ICQD), Hefei National Laboratory for Physical Sciences at the Microscale (HFNL), and Synergetic Innovation Center of Quantum Information and Quantum Physics, University of Science and Technology of China, Hefei, Anhui 230026, China*

[2]*Shenzhen Institutes of Advanced Technology, Chinese Academy of Sciences, Shenzhen 518055, China*

[3]*HFNL, University of Science and Technology of China, Hefei, Anhui 230026, China*

(Received 28 February 2014; revised manuscript received 24 September 2014; published 15 December 2014)

Superparamagnetism appears when the Néel-Brown relaxation time of magnetic nanoparticles is shorter than the measurement time. Recent experimental studies of different types of magnetic nanoparticles revealed the existence of another paramagnetic region below the standard blocking temperatures. Here we elucidate the microscopic origin of this reentrant paramagnetism using a phenomenological model, which exploits the effects of weaker magnetic coupling strengths at the surfaces of ultrasmall nanoparticles. Within this picture, we have calculated the total magnetization of various nanoparticle arrays upon both finite-field and zero-field cooling processes via detailed classical Monte Carlo simulations, and found that the appearance of the reentrant phenomena necessarily invokes a drastic reduction of the magnetic coupling strengths at the surfaces of the nanoparticles. Our predictions can be readily tested experimentally using a micro-SQUID, and is expected to be beneficial in further applications of superparamagnetic nanoparticles.

DOI: 10.1103/PhysRevB.90.224416 PACS number(s): 75.20.−g, 75.30.Gw, 75.50.Tt

I. INTRODUCTION

Magnetic nanoparticles have been widely studied for their potential applications in data storage [1–4], catalysis [5,6], biomedicine [7–9], nanofluids [10], and others. While bulk magnetic materials typically contain multiple magnetic domains, a magnetic nanoparticle will display a single domain behavior below a critical size. For a sufficiently small nanoparticle with a low anisotropy energy barrier, the thermal fluctuations could drive random flipping of the direction of the magnetic domain between different metastable states. This phenomenon is characterized by the Néel-Brown relaxation time, τ_N, which depends on the temperature as [11–13]

$$\tau_N = \tau_0 \exp\left(\frac{K_{an}V}{k_B T}\right), \tag{1}$$

where τ_0 is the typical time constant of the order 10^{-10}–10^{-12} s [13,14], K_{an} is the system-specific magnetic anisotropy parameter, V is the volume of the nanoparticle, k_B is the Boltzmann constant, and T is the temperature. When the measurement time τ_m is longer than τ_N, the magnetization of such a nanoparticle (or an assembly of such nanoparticles) will average to zero. This behavior, in analogy to the conventional paramagnetism of individual spins or magnetic moments, is described as superparamagnetism. On the other hand, if τ_m is shorter than τ_N, the thermally driven flipping of the total magnetic moment of the nanoparticle will be effectively frozen, and the corresponding superparamagnetic state is regarded as blocked, with a blocking temperature given by $T_B = K_{an}V/[k_B \ln(\tau_m/\tau_0)]$.

In early 2000, magnetization measurements in both Fe_3O_4 and $CoFe_2O_4$ nanoparticles revealed the existence of another paramagnetic region as the temperature continues to decrease to be substantially below the blocking temperature T_B [15]. Later, such reentrant paramagnetic phenomena have also been observed in diluted magnetic quantum dots of Cr-doped CdSe [16] and ultrasmall half-metallic V_3O_4 nanoparticles [17]. As summarized in Fig. 1, the reentrant paramagnetism is characterized by the appearance of a new paramagnetic phase at low temperatures. These peculiar observations have been interpreted in terms of macroscopic quantum tunneling (MQT) of the nanoparticle moments; and the phenomena are tentatively described as certain kinds of quantum phase transition within the systems [15,16]. However, an inherent contradiction with this interpretation can be found if considering earlier works by Chudnovsky and Tejada on MQT in magnetic nanoparticles [1,18]. In these studies, it was found that the relaxation time of the magnetic moment of a given nanoparticle at finite temperature is given by $\tau(T) = \tau_0 \exp[K_{an}V/k_B T^*(T)]$ with $T^*(T) = \max\{T, T_C\}$, where T_C is the crossover temperature from the thermal to the quantum regime [19,20]. Therefore, when T_C is lower than T_B, the relaxation time $\tau(T_C)$ in the quantum regime will be longer than the measurement time τ_m, indicating that the magnetic moments of the nanoparticles would be observed to be blocked; therefore the MQT of the magnetic nanoparticles cannot be responsible for the observed reentrant paramagnetic behavior.

In this article, a conceptually different phenomenological core-shell model for the superparamagnetic nanoparticles is introduced to provide an alternative physical origin for the reentrant paramagnetism. Within our new picture, a superparamagnetic nanoparticle is naturally divided into a core region with strong magnetic coupling and a shell region at the nanoparticle surface with weaker magnetic coupling. Detailed Monte Carlo (MC) simulations of total magnetization with the Wolff algorithm have been carried out to exploit the effects of

*Corresponding author: zhangzy@ustc.edu.cn

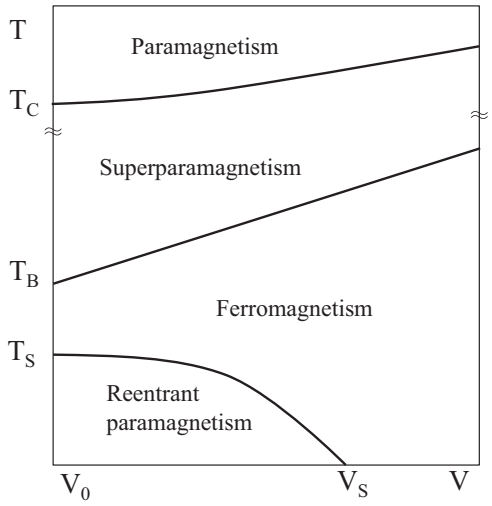

FIG. 1. Schematic phase diagram of a magnetic nanoparticle. The reentrant paramagnetic phase emerges when the size of the nanoparticle is small enough.

weaker magnetic coupling strength in the shell region for such systems [21]. Most notably, we find that the appearance of the reentrant phenomena necessarily invokes a drastic reduction of the magnetic coupling strength at the surfaces of magnetic nanoparticles. We have also systemically investigated the temperature dependence of the magnetization by varying the physical parameters of the nanoparticles, including their size, strength of the exchange coupling, and the magnetic anisotropy. Our predictions on the magnetization are expected to stimulate future experimental studies of different kinds of magnetic nanoparticles with ultrasmall sizes. In particular, in sharp contrast with the earlier quantum superparamagnetism picture, our present study implies the existence of a persistent ferromagnetic core accompanying the reentrant paramagnetism. This important finding can be readily tested experimentally using a micro-SQUID, and is expected to be beneficial in further applications of superparamagnetic nanoparticles.

The article is organized as follows: In Sec. II, we introduce the phenomenological core-shell model. We describe the numerical methods and computational details in Sec. III, where the Wolff MC algorithm is introduced to describe the formation and decomposition of large core clusters [21]. In Sec. IV, we present our main results of magnetization and coercivity from MC simulations. We find that a drastic reduction of magnetic coupling strengths at the surfaces will give rise to the appearance of reentrant behavior, which displays excellent agreement with the experimental observations. In addition, some intriguing observations in our simulations are also discussed. In Sec. V, we give a phenomenological description of the core-shell model, and systemically investigate the various physical parameters that control the reentrant phenomena, as presented in terms of different phase diagrams. In Sec. VI, we propose an experimental test of an important prediction made in the present study, and discuss the related technological benefits. Finally, we summarize our results in Sec. VII.

II. THEORETICAL MODELS

The reentrant paramagnetic phenomena reported experimentally invoked nanoparticle systems consisting of either transition-metal oxides or dilutely doped magnetic semiconductors [15–17,22]. Based on these experimental observations, we propose a phenomenological core-shell model that could qualitatively reproduce the experimental results and predict new aspects for further experimental tests.

The core-shell model contains several physically realistic assumptions: (1) Only the magnetic exchange coupling between two nearest magnetic cations is taken into account, while long-range magnetic dipole-dipole interaction is neglected. Typically, the magnetic exchange coupling in transition-metal oxides is indirect (through an intervening oxygen), and the strength of the coupling varies from several to tens of Kelvin [23]. On the other hand, it is straightforward to estimate the strength of magnetic dipole-dipole coupling in those materials. For example, the maximum summation of the dipole-dipole coupling is estimated to be $\sim$0.1 K for a 3-nm V_3O_4 (space group *Fd3m* and lattice constant $a = 8.457$ Å) nanoparticle, where the magnetic moment of the V^{3+} ion is assumed to be the typical value of 3.8 Bohr magnetons [24]. (2) The exchange coupling of two magnetic cations in the nanoparticle is spatially inhomogeneous, which shows a reduction in the surface region. There are several reasons to expect the reduction of magnetic coupling in the surface region of such magnetic nanoparticles [23]. First, since the superexchange interaction is mediated by an oxygen anion, the presence of oxygen vacancies in the surface region will naturally reduce the corresponding exchange coupling. Secondly, the surfaces of such nanoparticles are often decorated with foreign species whose valence electrons are less likely to participate in the superexchange progress. Thirdly, the superexchange coupling is very sensitive to both the bond angles and lengths, which would likely be modified near the surfaces, especially for ultrasmall nanoparticles. (3) The thickness of the surface region is taken as an input parameter, whose magnitude depends on the specific systems. (4) All the magnetic cations show uniaxial anisotropy.

Given the above core-shell picture, we could anticipate the following qualitative physical processes to evolve as the temperature gradually decreases. When the temperature is high enough, a single cation spin in either the surface region or the core region could be thermally excited to flip, characterizing the system to be in the normal paramagnetic state. When the temperature drops below the Curie temperature of the core, the spins in the core region will form a large cluster with a single magnetic moment, while the spins in the surface region are still in the paramagnetic state as a result of the weakened magnetic coupling strength. Although a single spin in the magnetic core cluster can no longer flip independently, the cluster could flip as a collective large effective spin if the thermal fluctuations within the system can overcome the anisotropy energy barrier, resulting in the superparamagnetic state of the core cluster. When the temperature further drops to be below the blocking temperature T_B of the core cluster, the magnetic core will be blocked in the ferromagnetic state. On the other hand, there exists another critical temperature, T_S, below which the surface spins can no longer be thermally excited and will join the core cluster to form a single-domain nanoparticle with

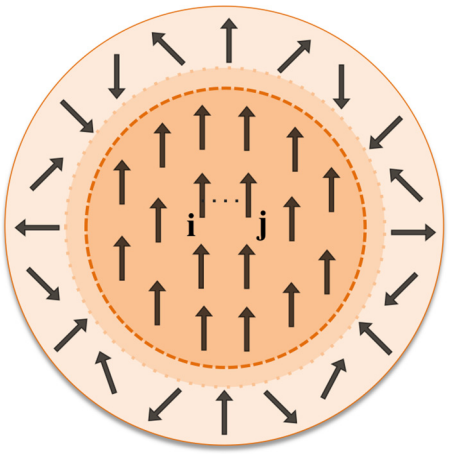

FIG. 2. (Color online) Schematic view of the spin configurations of a magnetic nanoparticle at finite temperatures, highlighting the coexistence of a ferromagnetic core and a paramagnetic surface region.

a maximum total magnetic moment. Qualitatively, a weaker magnetic coupling strength in the surface region would result in a lower T_S. If T_S is smaller than T_B, the ferromagnetic core and the paramagnetic surface region can coexist in the temperature range of T_S to T_B, as qualitatively illustrated in Fig. 2. In this regime, reentrant paramagnetic behavior may arise due to the existence of the paramagnetic surface region. In particular, since T_B is usually already quite small, the appearance of reentrant paramagnetic phenomena necessarily requires a drastic reduction of the magnetic coupling strength in the surface region of ultrasmall nanoparticles.

In our model, the Hamiltonian of a single magnetic nanoparticle is described as

$$H = -\sum_{ij} J_{ij}\vec{S}_i \cdot \vec{S}_j - \sum_i K_i\left(S_i^z\right)^2, \tag{2}$$

where $\vec{S}_i$ is the spin vector of cation i, K_i is the magnetic anisotropy parameter with easy magnetization along the z direction, and J_{ij} is the Heisenberg exchange coupling constant. In order to elucidate the effects of weaker magnetic coupling strength at the surface, we fix K_i for all magnetic cations. Although there may exist different magnetic anisotropy at the surfaces of real systems, such a simplified treatment will not affect the main results obtained in our present study. Based on the earlier descriptions of the model, the variation of J_{ij} with the site position r can be written as

$$J_{ij} = \begin{cases} J_C, & r \leqslant r_c \\ J_S, & r_c < r \leqslant R, \end{cases} \tag{3}$$

where R and r_c are the radius of the whole magnetic nanoparticle and the core region, respectively. For a given specific system, the distribution of J_{ij} may not be rigorously uniform in either the core or the surface region, and the transition between the two regions is unlikely to follow a step function, but inclusion of such finer differences will not alter the central physical picture to be revealed in the present study.

TABLE I. Typical nanoparticle size, lattice structure, blocking temperature (T_B), and crossover temperature (T_C) for several different kinds of magnetic nanoparticles previously investigated experimentally.

Material	Size (nm)	Structure	$T_B(K)$	$T_C(K)$	Reference
$CoFe_2O_4$	3	Inverse spinel	24	10	[15]
Fe_3O_4	3–5	Inverse spinel	35	16	[15]
CdCrSe	3.1	Wurtzite	300	20	[16]
V_3O_4	4.8	Inverse spinel	32	16	[17]

III. COMPUTATIONAL METHODS

It is presently unfeasible to analytically solve the many-body problem described by Eq. (2), even with the simplification of Eq. (3), but it can be systematically investigated numerically. Specifically, we adopt the Wolff cluster MC algorithm [21,25] to simulate the formation and flipping of the magnetic core cluster within the core-shell geometry. Details about the algorithm are presented in the Appendix. Given the magnetic anisotropy, we further restrict ourselves to the consideration of an Ising spin for each magnetic cation. The magnetic anisotropy is reflected by the existence of a transition state, such that each flipping between the up and down states must overcome the anisotropy energy barrier located at the transition state. The modification of the algorithm is presented in the Appendix.

The physical parameters used in our simulations are chosen to be comparable with the experimental data summarized in Table I. Specifically, the magnetic cations in the inverse spinel structured Fe_3O_4 and V_3O_4 nanoparticles form cubic structures (space group $Fd3m$) with lattice constants of 8.397 and 8.457 Å, respectively [15,17]. Furthermore, the superparamagnetic V_3O_4 nanoparticles were shown in transmission electron microscopy to adopt rough spherical geometry with diameters of about 3–6 nm following a Gaussian distribution [17]. It implies that a single nanoparticle contains roughly 1000 magnetic cations. We thus simulate a set of spherical nanoparticles with the simple cubic lattice structure and the average radius $R_0 = 6a$, where a is the simple cubic lattice constant. A Gaussian distribution $\frac{1}{\sigma\sqrt{2\pi}}\exp\left[-\frac{(R-R_0)^2}{2\sigma^2}\right]$ of the particle sizes has also been considered, with $\sigma = 0.6$ closely representing the experimental observations [17]. As described in Sec. II, a surface region with a thickness of $r_s = 3.1a$ has been introduced in our simulations. Typically, the bulk magnetic coupling strength of transition-metal oxides varies from several to tens of Kelvin. The corresponding Curie temperature is hundreds of Kelvin, which implies the core region of a given magnetic nanoparticle is tightly bounded together in the low temperature regime of our emphasis. In our simple cubic lattice case, the high Curie temperature cannot be obtained from realistic values of the magnetic coupling strength. In order to capture the central feature of a tightly bounded magnetic core cluster, we choose a large near-neighbor exchange coupling strength of $J_C = 100$ K to compensate the underestimation of the coupling strength due to the simplification of the lattice structure and ignorance of the coupling from the magnetic cations located further away. The resulting Curie temperature

TABLE II. Physical parameters used in the numerical simulations.

R_0 (a)	r_s (a)	J_C (K)	J_S (K)	K_{an} (K)	u (μ_B)
6.0	3.1	100	1.0–5.0	3.0	3.0

is ∼600 K as estimated from mean-field theory [26] and also typically observed experimentally [27]. We vary the magnetic coupling strength of the surface region, including much smaller values of $J_S = (1–5)$ K, to exploit the effects of drastic reductions of the magnetic coupling strength between the surface magnetic spins. More detailed discussions on the influence of the reentrant paramagnetism by varying J_S will be presented in Sec. V. The anisotropy parameter K_{an} is taken as 3 K per cation, which corresponds to 6.5×10^6 erg/cm^3, consistent with the experiment results [15,28–30]. We choose the typical value $u = 3.0\mu_B$ of a single cation moment in our simulations [24]. These parameters are also collectively summarized in Table II.

For the MC simulations, we have chosen $N = 3000$ noninteracting nanoparticles with a Gaussian size distribution to study the zero-field cooling (ZFC) and field cooling (FC) processes. For the ZFC process, we first demagnetized the samples at very high temperature and then cooled them down to the target low temperature of 3 K in zero applied magnetic field. During the heating, a small field of 500 G is applied and the magnetization is simulated. Both the heating and cooling rates are 0.5 K per every 10 000 MC steps. We have also studied the field dependence of the magnetization at different temperatures. Similarly, a high temperature demagnetization operation is necessary before the cooling process.

IV. MAGNETIZATION AND COERCIVITY FROM MC SIMULATIONS OF THE CORE-SHELL MODEL

Based on the core-shell model, we have simulated both the ZFC and FC magnetizations with various values of J_S. We found that, as long as J_S and J_C have comparable values, no reentrant paramagnetic ZFC behavior can be present; instead, standard superparamagnetism is obtained, characterized by the presence of a single magnetization maximum as the temperature decreases. More strikingly, we revealed that a drastic reduction of J_S is required for the appearance of the reentrant phenomena. Here we note that the experimental observation of reentrant paramagnetism in ultrasmall magnetic alloyed nanoparticles was interpreted using Metropolis MC simulations that also invoked a much weaker surface magnetic coupling strength than the core, even though such an assumption was built in implicitly [22]. Figure 3 presents the results for $J_S = 1.0$ K, which qualitatively agree with the experimental observations [15–17,22]. The ZFC curve exhibits a maximum at the blocking temperature T_B around 20 K, which marks the transition of the magnetic cores from the superparamagnetic to ferromagnetic states. The superposition of the ZFC and FC curves at the high temperature region indicates the reversible nature of the superparamagnetic behavior. The region below T_B is irreversible in its magnetization behavior, as indicated by the separation between the FC and ZFC curves. Furthermore, a distinct reentrant paramagnetic phase appears in the ZFC curve, which agrees well with the general trends

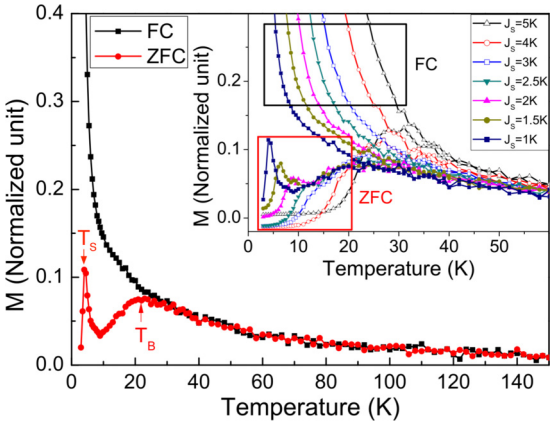

FIG. 3. (Color online) Temperature dependence of the magnetization for ZFC and FC processes, where $J_S = 1.0$ K. T_B and T_S in the ZFC curve indicate the blocking and saturation temperature, respectively. Inset: ZFC and FC curves of the magnetic nanoparticles with varying surface magnetic coupling strengths ranging from 1 to 5 K.

of the experimental observations [15,17,22]. There also exists another peak at 4.5 K, which is the critical temperature for the spins of the surface layer to start to align with the core cluster. The inset of Fig. 3 gives ZFC and FC curves with various magnetic coupling strengths J_S. By increasing J_S, we find that the reentrant behavior is gradually suppressed and finally completely embedded into the broad superparamagnetic peak, thus the appearance of the reentrant phenomena necessarily invokes a drastic reduction of the magnetic coupling strength at the surfaces of the nanoparticles.

To further support the above analysis for the ZFC and FC processes, we have simulated the magnetic field dependence of the magnetization. The results, measured at 100, 8, and 2 K after cooling the sample in zero field, are plotted in Fig. 4. The magnetization at 100 K shows no hysteresis indicating that all the magnetic nanoparticles are in the superparamagnetic state. In contrast, the significant hysteresis loops observed at 8 and 2 K demonstrate the existence of ferromagnetic components in the nanoparticles. As shown in Fig. 4, the remanence magnetization of the 2 K loop is about 6.5 times larger than that of the 8 K loop. This value is roughly equal to the ratio

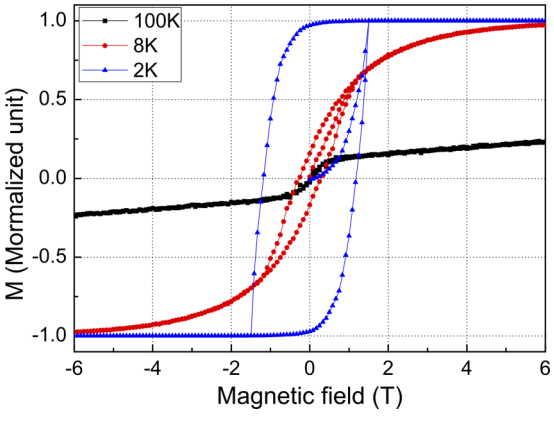

FIG. 4. (Color online) Hysteresis behaviors of the total magnetization as a function of the magnetic field at different temperatures.

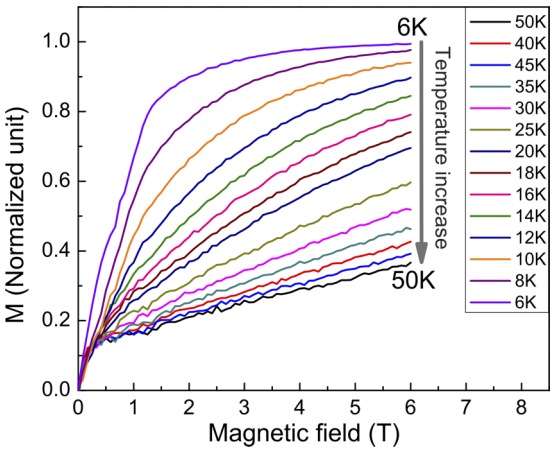

FIG. 5. (Color online) Saturation behaviors of the total magnetization as a function of the magnetic field at different temperatures.

of the total spins and core spins of the nanoparticles. The large increase of the remanence magnetization is consistent with our picture that the surface spins merge into the core cluster forming a larger ferromagnetic domain at extremely low temperatures.

The core-shell model also provides a temperature dependent saturation field of the magnetization, which has been observed in previous experimental studies [31–35]. In Fig. 5 we show the MH curves for temperature from 6 to 50 K. At the high magnetic field of 6 T, the total magnetization moment is smaller at higher temperatures, reflecting higher saturation fields rather than lower saturation moments as previously suggested [28]. The underlying physics is that unlike the core cluster, which saturates at a relatively low applied field, the surface spins are expected to achieve the saturation at a larger field, because the effective moment of those much more weakly coupled spins is much smaller than that of the core cluster [26].

We have further examined the temperature dependent coercive field, which can be easily compared with experimental measurements. In Fig. 6(a) we present the thermal dependence of the coercive field of singularly sized nanoparticles of radius $6a$. As the temperature decreases, the coercive field exhibits intriguing features: It first increases at relatively high temperatures, then decreases between 9 and 4 K, and increases again below 4 K. To understand these peculiar behaviors, we consider two coexisting contributions from the ferromagnetic core and paramagnetic surface region. The coercive field H_C of the monodomain core region can be well described by the Stoner-Wohlfarth model as [36]

$$H_C(T) = H_C(0)[1 - (T/T_B)^{1/2}]. \quad (4)$$

On the other hand, the magnetization of the surface paramagnetic region depends on the applied field h and temperature as [24]

$$M(h,T) = M_C L\left(\frac{\mu h}{k_B T}\right), \quad (5)$$

where $L(x) = \coth(x) - 1/x$ is the Langevin function, M_C is the total maximum magnetic moment of the spins in the surface region, and μ is the mean magnetic moment of a

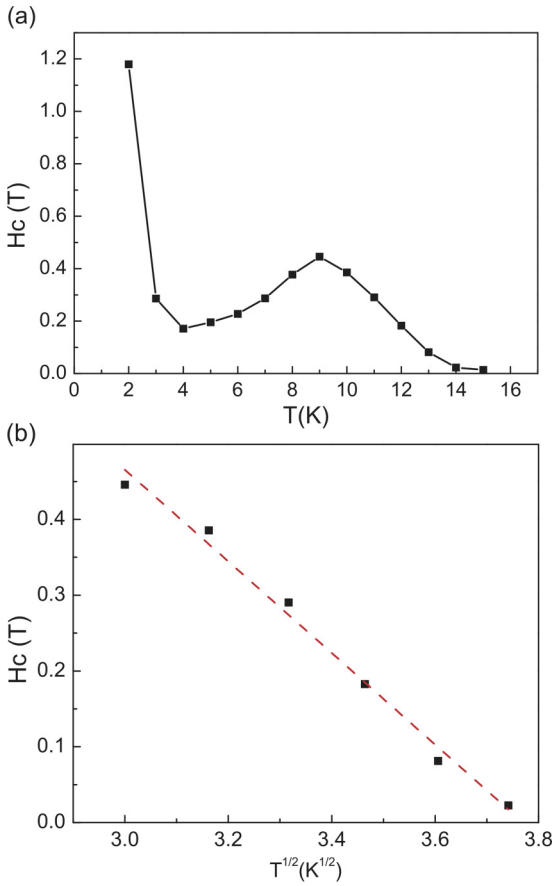

FIG. 6. (Color online) (a) Temperature dependence of the coercive field H_C. (b) Linear fitting of the coercive field H_C as a function of $T^{1/2}$ between the temperature range of 9 K and 14 K.

single thermodynamic statistical unit. At high temperatures, the surface magnetization is negligible and the coercive field mainly determined by Eq. (4) will increase as T drops. Further lowering the temperature, the surface magnetization becomes larger and non-negligible. The induced magnetic field in the surface region will help to increase the total magnetic field around the core, and effectively reduce the measured coercive field. As the temperature further decreases, the coercive field starts to increase again, because the surface spins saturate as they collectively merge into the core cluster. The blocking temperature $T_B = 14$ K is obtained from the linear fitting of the coercive field between 9 and 14 K by using the Stoner-Wohlfarth model in Fig. 6(b). We note that T_B here is lower than $T_B = 20$ K obtained earlier in Fig. 2, where the nanoparticle sizes satisfy a Gaussian distribution.

So far we have shown that excellent agreements between the experimental observations and simulated results can be obtained within the present core-shell model. In our simulations, one crucial finding is that the appearance of the reentrant phenomena necessarily invokes a drastic reduction of the magnetic coupling strengths at the surface region of the nanoparticles. In the following, we exploit other physical aspects and consequences based on this model, with the intension that such predictions can be further tested in future experiments.

V. REENTRANT PARAMAGNETISM FROM A PHENOMENOLOGICAL DESCRIPTION OF THE CORE-SHELL MODEL

In this section, we further explore the parameter space for observing the reentrant paramagnetic phenomena using a phenomenological description within the core-shell picture. We discuss mainly two physical parameters, the magnetic coupling strength J_S and the radius R of the magnetic nanoparticles. The condition to observe the reentrant phenomena is related to two quantities: the correlation length $\xi(T_B)$ between the core and surface spins at the blocking temperature T_B, and the thickness $d(R)$ of the surface layer for nanoparticles of radius R. Clearly, if $\xi(T_B)$ is larger than $d(R)$, we cannot observe the reentrant phenomena described above, because all the surface spins will be frozen into the core even above T_B. Conversely, if $\xi(T_B)$ is smaller than $d(R)$, the reentrant phenomena will appear. Therefore, the phase boundary can be evaluated from $\xi(T_B) = d(R)$.

We estimate the correlation length $\xi(T) = (\frac{J_S}{T-T_S})^{1/2}$ in units of the lattice constant a, and the Curie temperature of the surface layer to be $T_S = 2J_S D$, both from a mean-field description of a simple cubic lattice [26]. In these expressions, J_S is the magnetic coupling strength at the nanoparticle surface, and D is the physical dimension of the surface layer. Then, the phase boundary reads

$$J_S = \frac{1}{C}\frac{K_{an}V_{\text{eff}}(R)}{d^{-2}(R)+2D}, \tag{6}$$

where $C = \ln(\tau_m/\tau_N) \sim 25$ is a dimensionless constant, K_{an} is the anisotropy parameter in units of Kelvin, and $V_{\text{eff}} = \frac{4\pi}{3}[R-d(R)]^3$ is the effective volume of the nanoparticle which contributes to the blocking behavior. In Fig. 7 we show the phase boundary curves with different anisotropy parameters by taking $d(R) = 3.0a$. We find that the appearance of the reentrant phenomena demands a drastic reduction of the surface magnetic coupling strength J_S, and should be more readily observable for systems with larger anisotropy parameters.

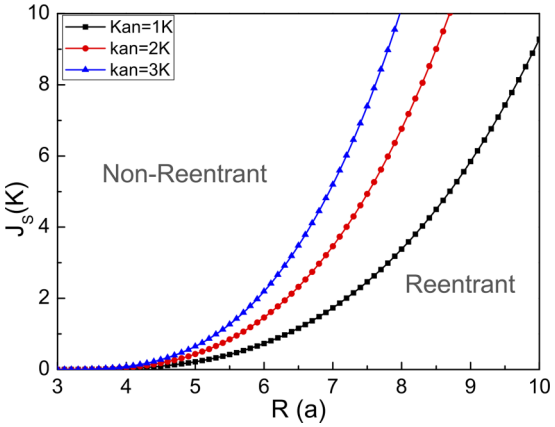

FIG. 7. (Color online) Parameter space spanned by the surface magnetic coupling strength J_S and magnetic nanoparticle radius R, in which the boundary separates the regions without (left) or with (right) the existence of the reentrant phenomena. The different curves correspond to different anisotropy parameters K_{an}.

For systems exhibiting the reentrant phenomena, we can also evaluate the relative magnitude (or the intensity for simplicity) of the reentrant magnetization $I(J_S,R)$, defined by the height of the reentrant magnetization peak around T_S as shown in Fig. 3. It is quite natural to note that the intensity is proportional to the total number of the surface spins as $I(R) \propto 1-[1-\frac{d(R)}{R}]^3$. For ZFC, when the temperature is far below T_S, the surface spins are ordered by the ferromagnetic core to form a single-domain nanoparticle, and the average magnetization will be zero because the magnetization directions of those nanoparticles are randomly distributed. As the temperature increases from T_S, the correlation length decreases and the spins in the surface layer are gradually activated. When the correlation length equals the lattice constant a, all the surface spins can flip in the external magnetic field without being ordered by the magnetic cores, providing the strongest intensity of the reentrant magnetization. From the mean-field results, the intensity maximum should be evaluated at $T_I = T_S + J_S$, and the magnetization of a simple cubic lattice in the presence of an external magnetic field could be described by the following self-consistent function:

$$m(h,T) = \tanh\left[\frac{h+T_S m(h,T)}{T}\right]. \tag{7}$$

By keeping only the first two Taylor expansion terms of $\tanh^{-1}(m)$ in Eq. (7), the solution at $T = T_I$ is

$$m(h,J_S) = \eta(h,J_S) - \frac{1}{7\eta(h,T)}, \tag{8}$$

with

$$\eta(h,J_S) = \frac{(2/7)^{1/3}J_S}{\left(-21hJ_S^2+\sqrt{7}\sqrt{63h^2J_S^4+4J_S^6}\right)^{1/3}}. \tag{9}$$

Therefore, the intensity of the reentrant magnetization can be expressed as

$$I(h,R,J_S) \approx \left[1-\left(1-\frac{d(R)}{R}\right)^3\right]\left[\eta(h,J_S)-\frac{1}{7\eta(h,T)}\right]. \tag{10}$$

As illustrated in Fig. 8, the intensity drops as the magnetic coupling strength increases, and the MC simulations shown as triangles display a good agreement with the prediction of Eq. (10).

In Fig. 9, we present the complete phase diagrams of the superparamagnetic nanoparticles based on our above discussions. The left boundary in each diagram indicates the valid region for the reentrant phenomena based on the analysis of the correlation length, and the density plots further give the intensity of the reentrant magnetization. Comparing Figs. 9(a) and 9(b), we find that the reentrant intensity shows an overall enhancement by increasing the external magnetic field.

Here we also briefly discuss the nanoparticle size dependence of the reentrant phenomena. First, there exists a critical size of the magnetic nanoparticle, below which the reentrant phenomena disappear. The critical radius $R_c = d + [3CJ_S(d^{-2}+2D)/4\pi K_{an}]^{1/3}$ can be derived from Eq. (6) with the thickness of the surface layer taken as a constant. In our MC simulations, the critical radius R_c is $3.1a$ while the

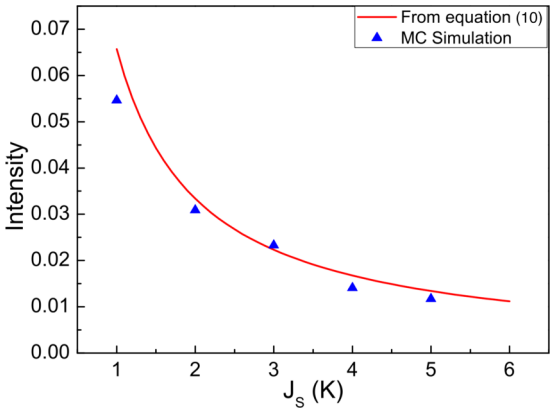

FIG. 8. (Color online) Intensity of the reentrant magnetization as a function of the surface magnetic coupling strength J_S, plotted with $R = 10a$, $d = 3.1a$, and $h = 0.05$ T.

coupling constant J_S is close to zero, resulting in $R_c \sim 1.24$ nm for the lattice constant around 4 Å. Secondly, as shown in Fig. 9, the reentrant phenomena shows a pronounced intensity at relatively small J_S even at large nanoparticle sizes. However, we note that when the size of the nanoparticle further increases, the surface contribution to the total magnetization becomes less and less significant compared to the core contribution, making the reentrant phenomena experimentally unobservable in practical conditions. Therefore, a distinct reentrant behavior can only have been experimentally observed in a size range of ultrasmall magnetic nanoparticles.

VI. PROPOSED EXPERIMENTAL TEST

In this section, we propose a definitive experimental measurement to reveal the microscopic mechanism of the reentrant phenomena. In order to avoid the complication due to the size distribution of nanoparticles, we propose to employ a single particle measurement technique based on micro-SQUID [37–39]. The experiment contains the following sequential steps: (a) Prepare magnetic nanoparticle samples and embed them into the microbridge Josephson junctions of the SQUID. (b) Cool the samples until the temperature reaches the reentrant regime in a strong magnetic field. This step aligns all the spins of a magnetic nanoparticle in a given direction. (c) Remove the external magnetic field and record the magnetization of a single nanoparticle in the zero magnetic field environment. The MQT picture would predict that the collective moment will flip in this reentrant regime, and the quantum relaxation time τ_q is shorter than the magnetization measurement time τ_m; therefore, the average magnetization would be zero. In contrast, the current core-shell model would naturally predict a finite average magnetization, because the Néel-Brown relaxation time τ_N of the core region is much longer than τ_m at $T < T_B$. The expected magnetization should be proportional to $\cos(\phi)$, where ϕ is the angle between the direction of the magnetization and the easy axis of the nanoparticle. The distinct difference between the predictions of the MQT picture and the core-shell model will serve as a decisive criterion for experimentally revealing the underlying physics involved in the reentrant paramagnetic phenomena.

For practical purposes, for example in memory devices, smaller particle sizes and longer spin relaxation times are the common pursuits. Within the MQT picture, the reentrant paramagnetic phenomena would destroy the ferromagnetic state below the blocking temperature T_B, leading to a lifetime shortening. In contrast, within the present core-shell picture, the reentrant paramagnetic phenomena coming from the contribution of the surface spins influence minimally on the magnetization behavior of the ferromagnetic cores. Therefore, the corresponding magnetic states will have a much longer lifetime. Furthermore, as the temperature continues to decrease, the surface spins will eventually merge with the ferromagnetic core, which will not only preserve but also strengthen the storage state.

VII. CONCLUSIONS

In summary, we have introduced a phenomenological core-shell model to describe the rich magnetization behaviors of ultrasmall magnetic nanoparticles, consisting of a core region with strong magnetic exchange coupling surrounded by a surface layer with weaker magnetic exchange coupling. Detailed MC simulations based on the Wolff algorithm well reproduce a series of low temperature behaviors of the superparamagnetic

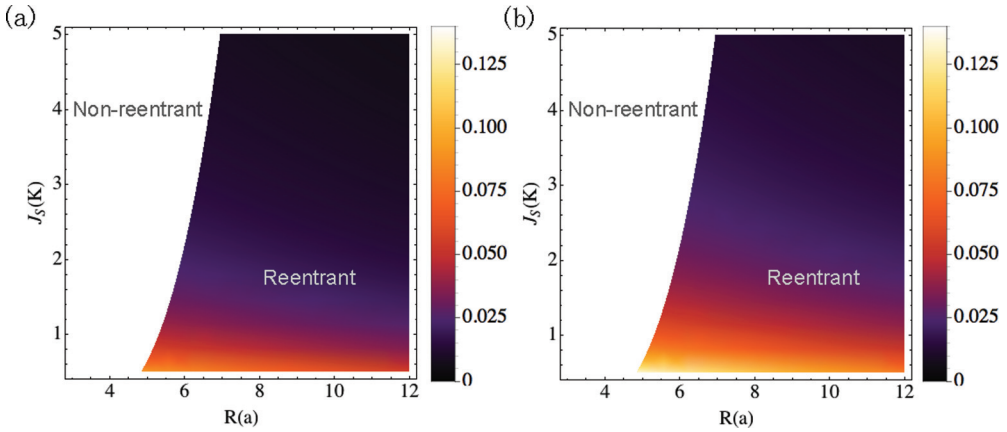

FIG. 9. (Color online) Intensity of the reentrant magnetization as a function of the surface magnetic coupling strength and magnetic nanoparticle radius, plotted with different external magnetic fields: (a) 0.05 T and (b) 0.075 T.

nanoparticles observed experimentally in various systems, allowing us to reveal the central physics involved. In particular, we found that the appearance of the reentrant phenomena necessarily demands a drastic reduction of the surface magnetic coupling strengths. The field dependence of the magnetization has been simulated at various temperatures. Robust hysteresis loops have been observed below the blocking temperature, and the existence of a much larger remanence magnetization at much lower temperatures indicates that all the surface spins have already merged into the magnetic core cluster. The magnetization evaluated at relatively high magnetic field decreases dramatically as the temperature increases, since the surface spins with drastically reduced magnetic coupling strengths are more difficult to be magnetized at high temperatures. The intriguing nonmonotonous behavior (first increasing, then deceasing, and increasing again) of the coercive field at low temperatures is respectively due to the magnetization and freezing of the surface spins in the external magnetic field. Furthermore, we have given a phenomenological description of the core-shell model and systemically investigated the physical parameter space for observing the reentrant phenomena. Consistent with the results of MC simulations, we have found that the phenomenologically predicted appearance of the reentrant phenomena also requires a drastic reduction of the magnetic coupling strength at the surfaces of the nanoparticles. The intensity of the reentrant magnetization will be suppressed by increasing the nanoparticle size and completely vanishes below a critical size. Therefore, the reentrant phenomena are only observable experimentally in a material-specific range of nanoparticle size, for example in systems with larger anisotropy parameters. Finally, we have proposed a definitive experimental test of the validity of the core-shell model by using micro-SQUID, and further discussed the related technological benefits in comparison with the prevailing quantum superparamagnetism picture.

ACKNOWLEDGMENTS

Discussions with Chong Xiao are greatly appreciated. This work was supported by National Natural Science Foundation of China (Grants No. 11034006 and No. 61434002), the National Key Basic Research Program of China (Grant No. 2014CB921103), and the Shenzhen Basic Research (Grant No. JCYJ20120831180435583).

APPENDIX

The Wolff prescription of MC simulations consists of the following steps: (a) Choose a random spin S_i at site i. (b) All nearest-neighbor spins S_j at sites j of the spin S_i are added to form a cluster with the probability

$$p_{ij} = 1 - \exp(\min[0, -2\beta J_{ij} S_i S_j]), \tag{A1}$$

provided that the bond between i and j has not been considered before, and J_{ij} is the coupling strength between S_i and S_j. (c) Scan iteratively all the bonds that have not been selected in step (b), as we determine the eventual size and total number of spins of a cluster. (d) All the spins belonging to the cluster are inverted together. We consider two configurations, $\{S_i\}$ and $\{S_i'\}$, which are connected by a single flip of the total spin of only one cluster C. The transition probability π obeys

$$\begin{aligned}\frac{\pi(\{S_i\} \to \{S_i'\})}{\pi(\{S_i'\} \to \{S_i\})} &= \prod_{\langle ij\rangle \in \partial C} \frac{(1 - p_{ij}) \exp(-\beta h M_c)}{(1 - p_{ij}') \exp(-\beta h M_c')} \\ &= \exp\left[\beta \sum_{\langle ij\rangle \in \partial C} (S_i S_j - S_i' S_j') \right. \\ &\quad \left. - \beta h \sum_{i \in C} (S_i - S_i')\right], \end{aligned} \tag{A2}$$

where the surface ∂C of the cluster C consists of all the links $\langle ij\rangle$ with $i \in C$ and $j \notin C$. Finally, the desired energy difference shown in the exponent of the last term of the above equation is obtained in a similar way as in the traditional Metropolis MC algorithm.

The appearance of the anisotropy energy will lead to a little modification of the Wolff algorithm. Similarly, when we consider the flipping of a total number of N_c spins in a magnetic core cluster, the corresponding transition rate contains a Boltzmann weight factor given by $\exp(-\beta h M_c - \beta \Delta E_{an})$, where h is the external magnetic field, M_c is the total moment, and $\Delta E_{an} \propto N_c K_{an}$ is the total anisotropy energy. The transition rates between two configurations $\{S_i\}$ and $\{S_i'\}$ can then be obtained as

$$\begin{aligned}\frac{\pi(\{S_i\} \to \{S_i'\})}{\pi(\{S_i'\} \to \{S_i\})} &= \prod_{\langle ij\rangle \in \partial C} \frac{(1 - p_{ij}) \exp(-\beta M_c h - \beta \Delta E_{an})}{(1 - p_{ij}') \exp(-\beta M_c' h - \beta \Delta E_{an}')} \\ &= \exp\left[\beta \sum_{\langle ij\rangle \in \partial C} (S_i S_j - S_i' S_j') \right. \\ &\quad \left. - \beta h \sum_{i \in C} (S_i - S_i')\right], \end{aligned} \tag{A3}$$

where the definitions of the different quantities can be found above. We note that Eq. (A3) is in essence similar to what is described in step (d) of the original Wolff algorithm.

[1] E. M. Chudnovsky and L. Gunther, Phys. Rev. Lett. **60**, 661 (1988).
[2] S. H. Sun, C. B. Murray, D. Weller, L. Folks, and A. Moser, Science **287**, 1989 (2000).
[3] V. Skumryev, S. Stoyanov, Y. Zhang, G. Hadjipanayis, D. Givord, and J. Nogués, Nature (London) **423**, 850 (2003).
[4] H. Zeng and S. H. Sun, Adv. Funct. Mater. **18**, 391 (2008).
[5] A.-H. Lu, W. Schmidt, N. Matoussevitch, H. Bönnemann, B. Spliethoff, B. Tesche, E. Bill, W. Kiefer, and F. Schüth, Angew. Chem., Int. Ed. **43**, 4303 (2004).
[6] S. C. Tsang, V. Caps, I. Paraskevas, D. Chadwick, and D. Thompsett, Angew. Chem. **116**, 5763 (2004).

[7] J. D. Hood, M. Bednarski, R. Frausto, S. Guccione, R. A. Reisfeld, R. Xiang, and D. A. Cheresh, Science **296**, 2404 (2002).
[8] A. K. Gupta and M. Gupta, Biomaterials **26**, 3995 (2005).
[9] X. M. Qian, X.-H. Peng, D. O. Ansari, Q. Q. Yin-Goen, G. Z. Chen, D. M. Shin, L. Yang, A. N. Young, M. D. Wang, and S. M. Nie, Nat. Biotechnol. **26**, 83 (2008).
[10] J. Philip, P. D. Shima, and B. Raj, Appl. Phys. Lett. **92**, 043108 (2008); Nanotechnology **19**, 305706 (2008).
[11] L. Néel, Ann. Geophys. **5**, 99 (1949).
[12] L. Néel, *Selected Works of Louis Neel* (Gordon and Breach, New York, 1988).
[13] W. F. Brown, Phys. Rev. **130**, 1677 (1963).
[14] C. Johansson, M. Hanson, P. V. Hendriksen, and S. Mørup, J. Magn. Magn. Mater. **122**, 125 (1993).
[15] C. T. Hsieh and J. T. Lue, Phys. Lett. A **300**, 636 (2002); **316**, 329 (2003).
[16] W. W. Zheng, P. Kumar, A. Washington, Z. X. Wang, N. S. Dalal, G. F. Strouse, and K. Singh, J. Am. Chem. Soc. **134**, 2172 (2012).
[17] C. Xiao, J. J. Zhang, J. Xu, W. Tong, B. X. Cao, K. Li, B. C. Pan, H. B. Su, and Y. Xie, Sci. Rep. **2**, 755 (2012).
[18] E. M. Chudnovsky and J. Tejada, *Macroscopic Quantum Tunneling of the Magnetic Moment* (Cambridge University Press, Cambridge, 1998).
[19] J. Tejada, X. X. Zhang, and E. M. Chudnovsky, Phys. Rev. B **47**, 14977 (1993).
[20] E. M. Chudnovsky, J. Appl. Phys. **73**, 6697 (1993).
[21] U. Wolff, Phys. Rev. Lett. **62**, 361 (1989).
[22] E. De Biasi, C. A. Ramos, R. D. Zysler, and H. Romero, Phys. Rev. B **65**, 144416 (2002).
[23] R. H. Kodama, A. E. Berkowitz, E. J. McNiff, Jr., and S. Foner, Phys. Rev. Lett. **77**, 394 (1996).
[24] C. Kittel, *Introduction to Solid State Physics* (Wiley, New York, 2005).
[25] R. H. Swendsen and J. S. Wang, Phys. Rev. Lett. **58**, 86 (1987).
[26] J. W. Negele and H. Orland, *Quantum Many Particle Systems* (Westview Press, Boulder, CO, 1988).
[27] M. W. Grinstaff, M. B. Salamon, and K. S. Suslick, Phys. Rev. B **48**, 269 (1993).
[28] G. F. Goya, T. S. Berquó, F. S. Fonseca, and M. P. Morales, J. Appl. Phys. **94**, 3520 (2003).
[29] C. T. Hsieh and J. T. Lue, Eur. Phys. J. B **35**, 357 (2003).
[30] J. M. D. Coey, Phys. Rev. Lett. **27**, 1140 (1971).
[31] E. Lima, Jr., E. D. Biasi, M. V. Mansilla, M. E. Saleta, F. Effenberg, L. M. Rossi, R. Cohen, H. R. Rechenberg, and R. D. Zysler, J. Appl. Phys. **108**, 103919 (2010).
[32] P. Hajra, M. Pal, A. Datta, D. Chakravorty, V. Meriakri, and M. Parkhomenko, J. Appl. Phys. **108**, 114306 (2010).
[33] S. Sharma, N. S. Gajbhiye, and R. S. Ningthoujam, J. Colloid Interface Sci. **351**, 323 (2010).
[34] T. Iwamoto, Y. Komorida, M. Mito, and A. Takahara, J. Colloid Interface Sci. **345**, 143 (2010).
[35] Y.-H. A. Wang, N. Z. Bao, L. M. Shen, P. Padhan, and A. Gupta, J. Am. Chem. Soc. **129**, 12408 (2007).
[36] E. C. Stoner and E. P. Wohlfarth, Philos. Trans. R. Soc. London **240**, 599 (1948).
[37] W. Wernsdorfer, E. B. Orozco, K. Hasselbach, A. Benoit, B. Barbara, N. Demoncy, A. Loiseau, H. Pascard, and D. Mailly, Phys. Rev. Lett. **78**, 1791 (1997).
[38] W. Wernsdorfer, D. Mailly, and A. Benoit, J. Appl. Phys. **87**, 5094 (2000).
[39] C. Thirion, W. Wernsdorfer, M. Jamet, V. Dupuis, P. Mélinon, A. Pérez, and D. Mailly, J. Magn. Magn. Mater. **242–245**, 993 (2002).